Theoretical insight into the electronic structures and photophysical properties of two series of iridium(III) complexes with different substitute groups or substituent position

JIAWEI LI[a], DEMING HAN[b,c], JING GAO[a], XIAOHONG SHANG[a,*]
aCollege of Chemistry and Life Science, Changchun University of Technology, Changchun 130012, P. R. China
bSchool of Life Science and Technology, Changchun University of Science and Technology, Changchun 130022, P. R. China
cJilin Provincial Science and Technology Innovation Center of Optical Materials and Chemistry, Changchun, 130022, P. R. China

The electronic structures and photophysical properties of two series of iridium(III) complexes have been investigated. Complexes **1b** and **2b** have the smallest IP values and the lowest hole injection energy barriers. The lowest energy absorptions for all studied complexes are assigned as the transition configurations of HOMO→LUMO. The calculated phosphorescence emission wavelength of complex **1** is in good agreement with the experiment value. The conclusion can be drawn that the different substituent group and substitution positions has obvious effect on the electronic structure and photophysical properties. The theoretical investigation will be useful to design new organic light-emitting diodes (OLEDs) material.

1. Introduction

In the recent two decades, organic light-emitting diodes (OLEDs) have attracted great interest due to the application for full-color flat-panel displays and low-cost lighting sources [1–6]. In transition metal complexes, the spin-orbit coupling (SOC) caused by heavy atoms accelerates the intersystem crossing (ISC) and triplet radiation decay, and promotes the $T_1 \rightarrow S_0$ transition of spin barrier. Therefore, as OLEDs materials, transition metal complexes with strong SOC are easy to form singlet and triplet excitons, and their maximum internal quantum efficiency can even be as high as 100% [7]. In particular, the cyclometalated metal Ir(III) complex has the high luminous efficiency and high thermal stability [8–12]. For example, Zhu *et al.* have successfully synthesized a series of homoleptic phosphorescent Ir(III) dendrimers by attaching the peripheral triphenylamine units to the different positions of the ligand frame in $Ir(ppy)_3$ [13]. It showed that the introduction of triphenylamine group leads to the enhancement of hole-transporting properties and remarkable color tuning abilities of these complexes.

Lin *et al.* have reported the photophysical properties of a novel class of heteroleptic Ir(III) complexes by incorporation of tripodal, facially coordinated phosphite (or phosphonate) [14]. On the basis of the synthesized complex from Lin *et al.* [14], we have theoretically investigated two series of iridium complexes in this study. The effect of different ligands on the photophysical properties of all designed complexes has been studied. It will be helpful to predict new and efficient phosphorescent materials for OLEDs.

2. Computational methods

The molecular structures of all studied complexes were optimized at the singlet ground state (S_0) and first triplet excited state (T_1) without symmetry constraints. The geometry of the S_0 state was optimized at the density functional theory (DFT) level using the hybrid-type Perdew–Burke–Ernzerhof exchange correlation functional (PBE0) [15]. The spin-unrestricted PBE0 (UPBE0) was adopted to optimize the structures of stable T_1 states. All the calculations of geometry optimization were performed using the 6–31G(d) basis set for C, H and N atoms and the "double-" quality LANL2DZ basis set [16,17] for the Ir element. A relativistic effective core potential (ECP)

replaces the inner core electrons of Ir, leaving the outer core $5s^2 5p^6$ electrons and the $5d^6$ as valence electrons of Ir(III). To obtain the absorption and emission spectral properties, time-dependent DFT (TDDFT) [18] calculations associated with the polarized continuum model (PCM) [19] in CH_2Cl_2 medium were performed on the basis of the optimized ground and the lowest triplet excited-state equilibrium geometries, respectively. The adopted PCM model is the integral equation formalism variant (IEFPCM), which creates the solute cavity via a set of overlapping spheres. All calculations were performed with the Gaussian 09 package [20]. GaussSum 2.5 program [21] was used for the orbitals manipulations and the ultraviolet–visible spectra analysis.

3. Results and discussion

3.1. Molecular geometries in the S_0 and T_1 states

The sketch map of two series of Ir(III) complexes (series 1, that is, **1**, **1a**, **1b** and **1c**; series 2, that is, **2**, **2a**, **2b** and **2c**) are presented in Fig. 1.
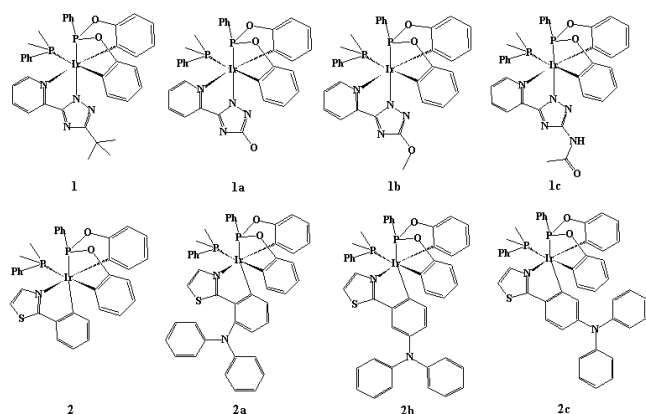
Fig. 1. Schematic structures of the investigated complexes

The optimized ground state geometric structure for **1** and **2** are also shown in Fig. 2 along with the numbering of some key atoms.

The main geometric parameters in the ground and lowest triplet states are summarized in Table S1 (Supporting Information). Fig. S1 (Supporting Information) has presented the names of different ligands in all studied complexes (taking complex **1** as an example), that is, L1, L2 and L3 ligands, respectively.

1

2
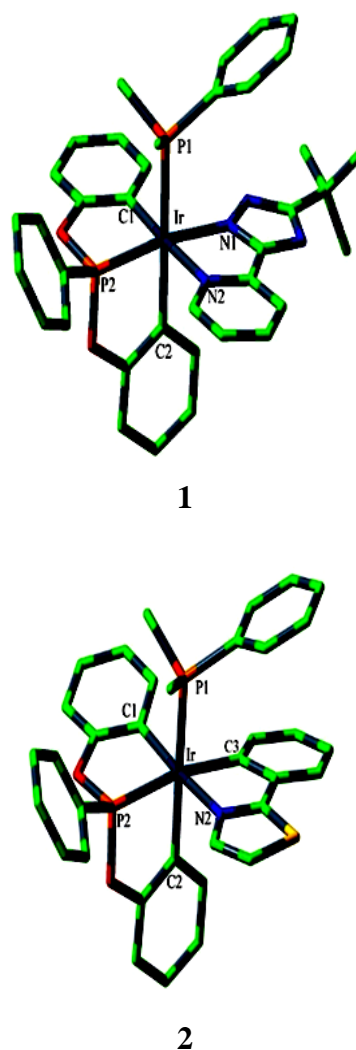
Fig. 2. Optimized geometry structures of 1 and 2 in the ground state (H atoms omitted) (color online)

It can be seen that the Ir–C1 bond lengths in series 1 complexes are identical, that is, 2.050 or 2.051 Å. The Ir–C2 bond lengths in complexes **1a**, **1b** and **1c** are slightly small than that of complex **1**. In series 1 complexes, the Ir–P1 and Ir–N2 bond lengths are obviously large than those of Ir–P2 and Ir–N1, respectively. In series 2 complexes, the Ir–C2 and Ir–P1 bond lengths are large than those of Ir–C1 and Ir–P2, respectively. The bond angles P1–Ir–C2 and C1–Ir–N2 for all studied complexes are larger than those of P2–Ir–N1/C3. For example, the bond angles P1–Ir–C2 and C1–Ir–N2 for complex **1** are 179.39° and 175.60°, respectively. However, the P2–Ir–N1 for **1** is only 169.24°. In addition, the bond angle P1–Ir–C1 values for all studied complexes are very close to 90°. Nevertheless, P1–Ir–P2 and C1–Ir–P2 have about 10° deviation from the right angle. For example, the P1–Ir–C1, P1–Ir–P2 and C1–Ir–P2 for complex **1** are 89.67°, 99.68° and 80.08°, respectively. The dihedral angles C1–N1/C3–N2–P2, C1–P1–N2–C2 and P1–P2–C2–N1/C3 for all studied complexes are very small and close to 0°. For example, the P1–P2–C2–N1 for

1 is 0.97°. Hence, from the optimized structure, it can be seen that all studied complexes have distorted octahedral configuration. From the S_0 to T_1 states, the bond length, bond angle and dihedral angle values for all studied complexes are slightly changed. For example, the dihedral angle P1–P2–C2–N1/C3 increases from the S_0 to T_1 states.

3.2. Frontier molecular orbital properties

The frontier molecular orbitals (FMOs) are directly related to the photophysical properties of these complexes. The energy levels of the highest occupied molecular orbitals (HOMO) and the lowest unoccupied molecular orbitals (LUMO) have been displayed in Fig. 3, along with the energy gaps between LUMO and HOMO ($\Delta E_{L \to H}$).
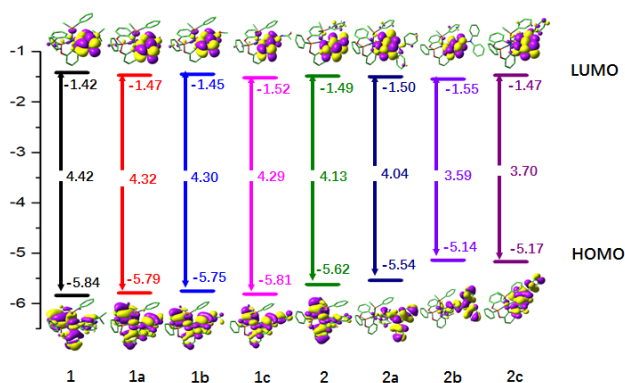
Fig. 3. Molecular orbital diagrams and HOMO and LUMO energies for all studied complexes (color online)

The detailed information of the molecular orbitals is collected in Tables S2–S9 (Supporting information).

It can be seen from Table S2–S5 and Fig. 3 that the HOMO distribution of series 1 complexes is mainly at the Ir atom, L1 and L3 ligands, however, the LUMO distribution of series 1 is mainly at the L3 ligand. For example, the HOMO for **1** is composed of 28% Ir d-orbital, 59% π-orbital of L1 ligand and 10% π-orbital of L3 ligand. The LUMO for **1** is composed of 92% π*-orbital of L3 ligand. For series 2 complexes, the HOMO and LUMO distribution is mainly on the L3 ligand, except the HOMO of **2**, that is, the 33% Ir d-orbital and 56% L1 π-orbital distribution. In contrast to 1, the HOMO and LUMO energy level of **1a**, **1b** and **1c** are slightly larger and smaller, respectively. The $\Delta E_{L \to H}$ values gradually decrease in the order 1→1a→1b→1c. As for series 2 complexes, in contrast to **2**, the HOMO energy levels of **2a**, **2b** and **2c** are larger. However, the LUMO energy levels of **2a** and **2b** slightly decrease. The $\Delta E_{L \to H}$ values of **2a**, **2b** and **2c** are obviously smaller than that of **2**. It can be seen that the different substituent positions of diphenylamine unit have a significant effect on the molecular orbital energy levels and $\Delta E_{L \to H}$, which would make it feasible to tune the photophysical properties of these complexes.

3.3. Ionization Potential (IP) and Electron Affinity (EA)

The performance of an OLEDs device is primarily determined by charge injection, transfer and balance ability. Ionization potential (IP) and electron affinity (EA) can be used to predict the energy barrier of holes and electrons. At the same time, IP and EA can be vertical excitation (v, at the geometry of neutral molecule) or adiabatic excitation (a, using optimized ground state and charged molecules). The calculated vertical IP (IP_v), adiabatic IP (IP_a), vertical EA (EA_v), and adiabatic EA (EA_a) are listed in Table 1.

Table 1. Ionization potentials, electron affinities, extraction potentials, internal reorganization energies and $\Delta = |\lambda_h - \lambda_e|$ (in eV) for all studied complexes

	IP_v	IP_a	HEP	EA_v	EA_a	EEP	λ_h	λ_e	Δ
1	5.71	5.48	5.48	1.50	1.84	1.84	0.23	0.34	0.11
1a	5.67	5.47	5.47	1.55	1.72	1.72	0.20	0.18	0.02
1b	5.64	5.46	5.16	1.59	1.70	1.70	0.18	0.10	0.08
1c	5.69	5.50	5.50	1.60	1.77	1.77	0.19	0.17	0.02
2	5.46	5.24	5.24	1.60	1.77	1.77	0.22	0.17	0.05
2a	5.42	5.25	5.25	1.61	1.79	1.79	0.18	0.18	0.00
2b	5.01	4.89	4.89	1.66	1.86	1.86	0.12	0.20	0.08
2c	5.40	4.97	4.97	1.59	1.84	1.84	0.06	0.25	0.19

A small IP (large EA) means that the holes (electrons) are easy to inject into emitter from the anode (cathode), thus the turn-on voltage is low and the performance of devices is good. **1b** and **2b** have the smallest IP values, so their hole injection energy barriers are the lowest ones in the series 1 and 2 complexes, respectively. In addition, **2b** has the largest EA values in the series 2 complexes.

According to the semi-empirical Marcus–Hush model [22–24], the transfer rate of charge (holes and electrons) K_{et} can be expressed by the following formula:

$$K_{et} = A\exp(-\lambda/4K_B T) \qquad (1)$$

where λ is the reorganization energy, A is the electron coupling correlation factor between adjacent molecules, and T and k_B are the temperature and Boltzmann constant, respectively. Due to the limited intermolecular charge transfer range in solid state, the mobility of charges has been demonstrated to predominantly relate to the internal reorganization energy λ for OLEDs materials [25–28]. According to the formula (1), at a certain temperature, the smaller the λ value is, the faster the charge transfer rate is.

In general, λ is determined by fast changes in molecular geometry (the internal reorganization energy λ_i) and by slow variations in solvent polarization of the surrounding medium (the external reorganization energy

λ_e). In OLEDs devices, the contribution from λ_e can be neglected. Therefore, here we will mainly discuss the internal reorganization energy of the complex.

$$\lambda_i = \lambda_0 + \lambda_1 = \left(E_B^A - E_A\right) + \left(E_B^A - E_B\right) \quad (2)$$

Among them, E_A and E_A^B are the energy of A and B in the balanced configuration of A, respectively, while E_B^A and E_B are the energy of A and B in the balanced configuration of B, respectively. In addition, we also calculated the extraction energy of the holes (HEP) and electrons (EEP) of the complex at the same theoretical level. HEP is the energy difference between the neutral molecule M and the cation M^+ in the equilibrium configuration of M^+. EEP is the energy difference between the neutral molecule M and the anion M^- in the equilibrium configuration of M^-. As can be seen from Fig. 4, the reorganization energy of hole transport (λ_h) and electron transport (λ_e) can be expressed by the following formula [29]:

$$\lambda_h = IP_v - HEP \quad (3)$$

$$\lambda_e = EEP - EA_v \quad (4)$$
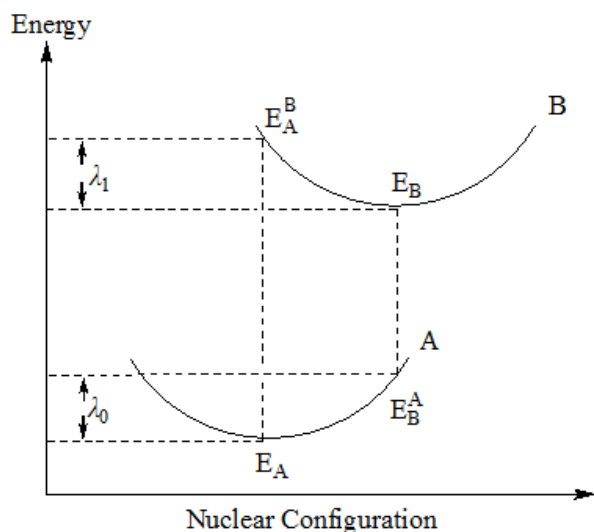
Fig. 4. Schematic description of the inner reorganization energy

Table 1 lists the reorganization energies of hole and electron transport for all studied complexes. λ_h and λ_e can be used to estimate the transport rate and equilibrium ability of charge. **1b** and **2c** have the best hole transfer ability with the smallest λ_h values in series 1 and 2 complexes. In addition, the difference between λ_e and λ_h for **2a** is the smallest one among all studied complexes, which can greatly improve the charge transfer balance, thus further enhancing the device performance of OLEDs. It can be found that changing the substituent group and substitution position in these complexes will result in

some effect on the charge transfer properties.

3.4. Absorption spectra

On the basis of the optimized ground state geometries, the absorption properties of all studied complexes have been calculated from the TDDFT/PBE0/LANL2DZ/6–31G(d) level. The vertical electronic excitation energies, oscillator strengths (*f*), dominant configurations and their assignments of singlet excited states have been listed in Table S10 (Supporting information). Meanwhile, the simulated absorption curves of all studied complexes in CH_2Cl_2 medium are presented in Fig. 5.
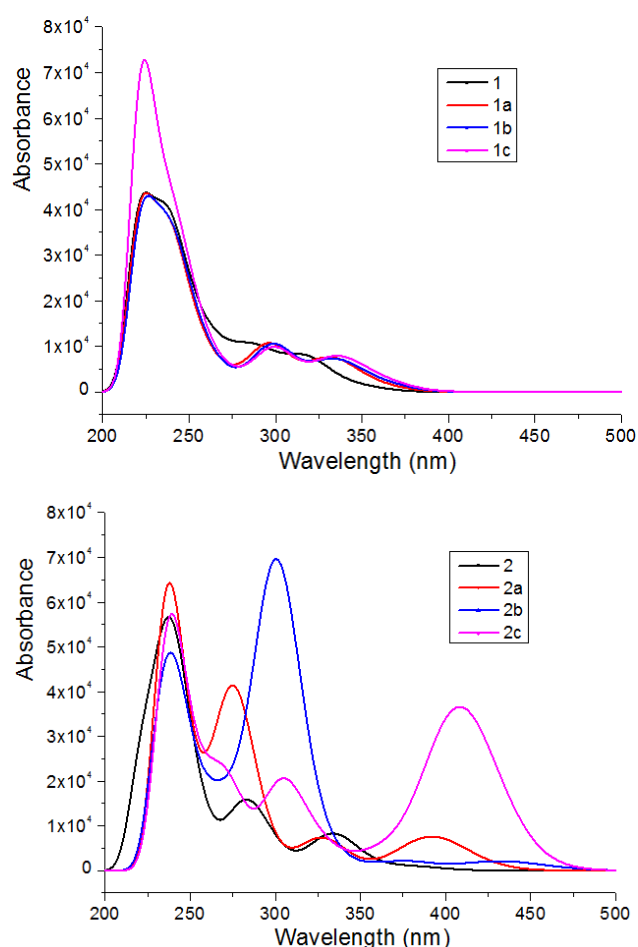
Fig. 5. Absorption spectra for in CH_2Cl_2 medium for all studied complexes (color online)

In series 1 complexes, **1** has the obvious strong absorption peak in contrast to those of other three complexes. Complexes **1a**, **1b** and **1c** have the similar absorption curve shape and very close absorption peak. The four complexes in series 2 have the different absorption curves and the strongest absorption at about 230 nm. These lowest lying transitions for all studied complexes are attributed to the configurations of

HOMO→LUMO. The calculated lowest lying absorption 329 nm for complex **1** is comparable to the experimental value [14]. In series 1 complexes, the lowest lying absorption of **1a**, **1b** and **1c** are very close and slightly redshifted in contrast to that of complex **1**. The lowest lying absorption of four complexes in series 1 have the same transition characters, that is, $d(Ir)+\pi(L1+L3)\rightarrow\pi^*(L3)$, which can be characterized as metal to ligand charge transfer (MLCT)/ligand-to-ligand charge transfer (LLCT)/intraligand charge transfer (ILCT). Complex **1c** has the strongest absorption peak at the wavelength 225 nm. In series 2 complex, the lowest lying absorption of **2a**, **2b** and **2c** are very obviously redshifted in contrast to that of complex **2**. The lowest lying absorption of complexes **2a**, **2b** and **2c** have the same

transition characters, that is, ILCT/[$\pi(L3)\rightarrow\pi^*(L3)$]. However, the lowest lying absorption of **2** has the different transition character, that is, MLCT/LLCT/[$d(Ir)+\pi(L1)\rightarrow\pi^*(L3)$]. Especially, **2b** has the largest absorption peak at 301 nm wavelength.

3.5. Phosphorescence in CH_2Cl_2 medium

In order to accurately predict the phosphorescence spectral properties of all studied complexes, we used TDDFT/M06HF functional to calculate the emission wavelength of complex **1**. The calculated results and corresponding experimental values are listed in Table 2.

Table 2. The calculated emission wavelength (nm) in CH_2Cl_2 medium at the TDDFT/M06HF level, along with the major contribution and transition characters

	λ(nm)/E(eV)	Configuration	Assignment	Nature	Exptl.[a]
1	446/2.77	H→L (87%)	$d(Ir)+\pi(L1+L3)\rightarrow\pi^*(L3)$	^{3}MLCT/^{3}ILCT/^{3}LLCT	454
1a	490/2.52	H→L (88%)	$d(Ir)+\pi(L3)\rightarrow\pi^*(L3)$	^{3}MLCT/^{3}ILCT	
1b	495/2.50	H→L (88%)	$\pi(L3)\rightarrow\pi^*(L3)$	^{3}ILCT	
1c	485/2.55	H→L (85%)	$\pi(L3)\rightarrow\pi^*(L3)$	^{3}ILCT	
2	538/2.30	H→L (92%)	$d(Ir)+\pi(L1+L3)\rightarrow\pi^*(L3)$	^{3}MLCT/^{3}ILCT/^{3}LLCT	
2a	523/2.37	H-1→L (46%)	$d(Ir)+\pi(L1+L3)\rightarrow\pi^*(L3)$	^{3}MLCT/^{3}ILCT/^{3}LLCT	
		H→L (42%)	$d(Ir)+\pi(L1+L3)\rightarrow\pi^*(L3)$	^{3}MLCT/^{3}ILCT/^{3}LLCT	
2b	512/2.42	H-2→L (19%)	$\pi(L1)\rightarrow\pi^*(L3)$	^{3}LLCT	
		H→L (66%)	$\pi(L3)\rightarrow\pi^*(L3)$	^{3}ILCT	
2c	576/2.15	H-3→L (12%)	$d(Ir)+\pi(L1+L3)\rightarrow\pi^*(L3)$	^{3}MLCT/^{3}ILCT/^{3}LLCT	
		H→L (81%)	$\pi(L3)\rightarrow\pi^*(L3)$	^{3}ILCT	

[a] Ref. [14]

The wavelength 446 nm of the complex **1** obtained using the TDDFT/M06HF level is in good agreement with the experimental value [14]. Therefore, we will further calculate the phosphorescence spectral properties of all other complexes using the TDDFT/M06HF method.

In contrast to that of complex **1**, the emission wavelengths of **1a**, **1b** and **1c** are obviously redshifted, which indicates that the addition of different auxiliary ligands will significantly affect the properties of the emission spectra of these complexes. The emission wavelengths of series 1 complexes have the same transition configuration HOMO→LUMO. For example, the transition character of the lowest energy emission for complex **1** has the HOMO→LUMO (87%) transition configuration. Compared with **2**, the emission wavelengths of **2a** and **2b** are blueshifted, however, the emission wavelength of **2c** is redshifted. The emission transition characters of series 2 complexes are different. For example,

the emission transition characters of **2** is assigned to ^{3}MLCT (triplet metal to ligand charge transfer)/^{3}LLCT (triplet ligand to ligand charge transfer)/^{3}ILCT (triplet intraligand charge transfer) [$d(Ir)+\pi(L1+L3)\rightarrow\pi^*(L3)$]. From Table S11 (Supporting information), it can be seen that the HOMO and LUMO in the T_1 state for **1a**, **1b** and **1c** are mainly distributed at the L3 ligand. However, the HOMO distribution in the T_1 state for **1** is located at 20% Ir d-orbital, 29% π-orbital of L1 ligand and 48% π-orbital of L3 ligand. In addition, the LUMO distribution in the T_1 state for series 2 complexes also mainly locate at the L3 ligand.

4. Conclusion

The geometrical structures, electronic structures, absorption and phosphorescent properties of two series of

iridium(III) complexes have been theoretically studied by using the DFT/TDDFT method. The HOMO distribution of series 1 complexes mainly locates at the Ir atom, L1 and L3 ligands. Nevertheless, the LUMO of series 1 mainly distributes at the L3 ligand. The energy difference between λ_h and λ_e for complex **2a** is the smallest one among all studied complexes, resulting in the good charge transfer balance. The calculated lowest lying absorption for complex **1** can be comparable to the experimental datum. The lowest lying absorption of **2a**, **2b** and **2c** have the ILCT/[π(L3)→π*(L3)] transition characters. However, **2** has the MLCT/LLCT/[d(Ir)+π(L1)→π*(L3)] transition character. The HOMO and LUMO distributions in the T$_1$ state for **1a**, **1b** and **1c** are mainly located at the L3 ligand. It can be seen that the different substituent group and substitution positions will result in different effect on the electronic structure and photophysical properties of all studied complexes. We hope these theoretical results would be useful for the design and synthesis of novel phosphorescent OLEDs materials in the future.

References

[1] Y. H. Sun, X. L. Yang, B. A. Liu, J. S. Dang, Y. Li, G. J. Zhou, Z. X. Wu, W. Y. Wong, J. Mater. Chem. C **7**, 8836 (2019).

[2] V. Adamovich, S. Bajo, P. L. T. Boudreault, M. A. Esteruelas, A. M. Lopez, J. Martin, M. Olivan, E. Onate, A. U. Palacios, A. San-Torcuato, J. Y. Tsai, C. J. Xia, Inorg. Chem. **57**, 10744 (2018).

[3] A. Maheshwaran, V. G. Sree, H. Y. Park, H. Kim, S. H. Han, J. Y. Lee, S. H. Jin, Adv. Funct. Mater. **28**, 1802945 (2018).

[4] D. M. Han, P. Gong, S. H. Lv, L. H. Zhao, H. N. Zhao, Mol. Phys. **116**, 1218 (2018).

[5] B. Y. Song, Y. Zhou, H. M. Yang, J. H. Liao, L. M. Yang, X. B. Yang, E. Ganz, J. Am. Chem. Soc. **141**, 3630 (2019).

[6] L. M. Yang, V. Bacic, I. A. Popov, A. I. Boldyrev, T. Heine, T. Frauenheim, E. Ganz, J. Am. Chem. Soc. **137**, 2757 (2015).

[7] M. A. Baldo, D. F. O'Brien, Y. You, A. Shoustikov, S. Sibley, M. E. Thompson, S. R. Forrest, Nature **395**, 151 (1998).

[8] X. F. Ma, J. C. Xia, Z. P. Yan, X. F. Luo, Z. G. Wu, Y. X. Zheng, W. W. Zhang, J. Mater. Chem. C **7**, 2570 (2019).

[9] Y. H. Zhou, D. Jiang, Y. X. Zheng, J. Organomet. Chem. **876**, 26 (2018).

[10] G. Sarada, W. Cho, A. Maheshwaran, V. G. Sree, H. Y. Park, Y. S. Gal, M. Song, S. H. Jin, Adv. Funct. Mater. **27**, 1701002 (2017).

[11] D. Liu, L. J. Deng, W. Li, R. J. Yao, D. L. Li, M. Wang, S. F. Zhang, Adv. Optical Mater. **4**, 864 (2016).

[12] J. Hwang, K. S. Yook, J. Y. Lee, Y. H. Kim, Dyes Pigments **121**, 73 (2015).

[13] M. R. Zhu, Y. H. Li, B. Jiang, S. L. Gong, H. B. Wu, J. G. Qin, Y. Cao, C. L. Yang, Org. Electron. **26**, 400 (2015).

[14] C. H. Lin, Y. Y. Chang, J. Y. Hung, C. Y. Lin, Y. Chi, M. W. Chung, C. L. Lin, P. T. Chou, G. H. Lee, C. H. Chang, W. C. Lin, Angew. Chem. Int. Ed. **50**, 3182 (2011).

[15] J. P. Perdew, K. Burke, M. Ernzerhof, Phys. Rev. Lett. **80**, 891 (1998).

[16] P. J. Hay, W. R. Wadt, J. Chem. Phys. **82**, 270 (1985).

[17] P. J. Hay, W. R. Wadt, J. Chem. Phys. **82**, 299 (1985).

[18] T. Helgaker, P. Jørgemsen, J. Chem. Phys. **95**, 2595 (1991).

[19] R. Baer, Chem. Phys. Lett. **364**, 75 (2002).

[20] M. J. Frisch, G. W. Trucks, H. B. Schlegel, G. E. Scuseria, M. A. Robb, J. R. Cheeseman, G. Scalmani, V. Barone, B. Mennucci, G. A. Petersson, H. Nakatsuji, M. Caricato, X. Li, H. P. Hratchian, A. F. Izmaylov, J. Bloino, G. Zheng, J. L. Sonnenberg, M. Hada, M. Ehara, K. Toyota, R. Fukuda, J. Hasegawa, M. Ishida, T. Nakajima, Y. Honda, O. Kitao, H. Nakai, T. Vreven, J. A. Montgomery Jr., J. E. Peralta, F. Ogliaro, M. Bearpark, J. J. Heyd, E. Brothers, K. N. Kudin, V. N. Staroverov, R. Kobayashi, J. Normand, K. Raghavachari, A. Rendell, J. C. Burant, S. S. Iyengar, J. Tomasi, M. Cossi, N. Rega, J. M. Millam, M. Klene, J. E. Knox, J. B. Cross, V. Bakken, C. Adamo, J. Jaramillo, R. Gomperts, R. E. Stratmann, O. Yazyev, A. J. Austin, R. Cammi, C. Pomelli, J. W. Ochterski, R. L. Martin, K. Morokuma, V. G. Zakrzewski, G. A. Voth, P. Salvador, J. J. Dannenberg, S. Dapprich, A. D. Daniels, O. Farkas, J. B. Foresman, J. V. Ortiz, J. Cioslowski, D. J. Fox, Gaussian 09, Revision A.1, Gaussian, Inc, Wallingford CT, 2009.

[21] N. M. O'Boyle, A. L. Tenderholt, K. M. Langner, J. Comput. Chem. **29**, 839 (2008).

[22] N. S. Hush, J. Chem. Phys. **28**, 962 (1958).

[23] R. A. Marcus, Rev. Mod. Phys. **65**, 599 (1993).

[24] R. A. Marcus, J. Chem. Phys. **24**, 966 (1956).

[25] M. Malagoli, J. L. Brédas, Chem. Phys. Lett. **327**, 13 (2000).

[26] B. C. Lin, C. P. Cheng, Z. Ping, M. Lao, J. Phys. Chem. A **107**, 5241 (2003).

[27] K. Sakanoue, M. Motoda, M. Sugimoto, S. Sakaki, J. Phys. Chem. A **103**, 5551 (1999).

[28] Y. Z. Lee, X. W. Chen, S. A. Chen, P. K. Wei, W. S. Fann, J. Am. Chem. Soc. **123**, 2296 (2001).

[29] G. R. Hutchison, M. A. Ratner, T. J. Marks, J. Am. Chem. Soc. **127**, 2339 (2005).

_____

*Corresponding author: shangxiaohong58@aliyun.com